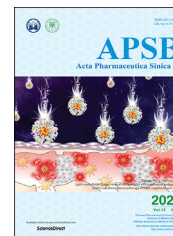




Chinese Pharmaceutical Association
Institute of Materia Medica, Chinese Academy of Medical Sciences

Acta Pharmaceutica Sinica B

www.elsevier.com/locate/apsb
www.sciencedirect.com



ORIGINAL ARTICLE

Atractylenolide-I covalently binds to CYP11B2, selectively inhibits aldosterone synthesis, and improves hyperaldosteronism



Wenjuan Liu^a, Zhenqiang Li^a, Simeng Chu^a, Xiaoyao Ma^a,
Xiaoying Wang^b, Min Jiang^{a,*}, Gang Bai^{a,*}

^aState Key Laboratory of Medicinal Chemical Biology, College of Pharmacy and Tianjin Key Laboratory of Molecular Drug Research, Nankai University, Tianjin 300353, China

^bTianjin University of Traditional Chinese Medicine, Tianjin 300193, China

Received 25 May 2021; received in revised form 10 August 2021; accepted 31 August 2021

KEY WORDS

Aldosterone;
CYP11B2;
Hyperaldosteronism;
Atractylenolide-I;
Selective inhibitor

Abstract Hyperaldosteronism is a common disease that is closely related to endocrine hypertension and other cardiovascular diseases. Cytochrome P450 11B2 (CYP11B2), an important enzyme in aldosterone (ALD) synthesis, is a promising target for the treatment of hyperaldosteronism. However, selective inhibitors targeting CYP11B2 are still lacking due to the high similarity with CYP11B1. In this study, atractylenolide-I (AT-I) was found to significantly reduce the production of ALD but had no effect on cortisol synthesis, which is catalyzed by CYP11B1. Chemical biology studies revealed that due to the presence of Ala320, AT-I is selectively bound to the catalytic pocket of CYP11B2, and the C8/C9 double bond of AT-I can be epoxidized, which then undergoes nucleophilic addition with the sulfhydryl group of Cys450 in CYP11B2. The covalent binding of AT-I disrupts the interaction between heme and CYP11B2 and inactivates CYP11B2, leading to the suppression of ALD synthesis; AT-I shows a significant therapeutic effect for improving hyperaldosteronism.

© 2022 Chinese Pharmaceutical Association and Institute of Materia Medica, Chinese Academy of Medical Sciences. Production and hosting by Elsevier B.V. This is an open access article under the CC BY-NC-ND license (<http://creativecommons.org/licenses/by-nc-nd/4.0/>).

*Corresponding authors. Tel./fax: +86 22 23506930.

E-mail addresses: gangbai@nankai.edu.cn (Gang Bai), minjiang@nankai.edu.cn (Min Jiang).

Peer review under responsibility of Chinese Pharmaceutical Association and Institute of Materia Medica, Chinese Academy of Medical Sciences.

<https://doi.org/10.1016/j.apsb.2021.09.013>

2211-3835 © 2022 Chinese Pharmaceutical Association and Institute of Materia Medica, Chinese Academy of Medical Sciences. Production and hosting by Elsevier B.V. This is an open access article under the CC BY-NC-ND license (<http://creativecommons.org/licenses/by-nc-nd/4.0/>).

1. Introduction

Aldosterone (ALD), a mineralocorticoid steroid hormone produced by the adrenal gland, is involved in electrolyte and volume homeostasis^{1,2}. Hyperaldosteronism is produced by the secretion of excess ALD from the adrenal cortex, resulting in the retention of sodium and potassium excretion, increased blood volume, and renin–angiotensin system activity, leading to many diseases^{3–6}. It is one of the most common causes of endocrine hypertension, accounting for 6%–10% of patients with hypertension, and is associated with a significant increase in morbidity and mortality^{7–10}. Hyperaldosteronism is also associated with insulin resistance and accelerates the progression of metabolic syndrome^{11,12}. The resulting increase in cardiovascular and renal disorders can cause heart failure, ischemic heart disease, arrhythmias, stroke, and kidney disease.

Owing to the negative consequences of excessive ALD levels, research on inhibiting ALD production has attracted much attention recently. ALD is synthesized under the strict control of the renin–angiotensin–aldosterone system (RAAS) and promotes sodium and water reabsorption by activating the mineralocorticoid receptor (MR)^{13–15}. Hence, two main pharmacotherapies are clinically implemented for the treatment of hyperaldosteronism, including RAAS inhibitors and MR antagonists. In the case of RAAS inhibition, a reduction in ALD levels is realized initially; however, this reduction is not maintained because of the phenomenon known as “aldosterone escape”^{16,17}. The MR antagonists can effectively block ALD binding to MR. However, due to their steroidal structure and lack of selectivity relative to other steroid receptors, they have some undesired effects in clinical application^{18,19}. Thus, the discovery of new inhibitors that directly inhibit the production of ALD would be beneficial for the treatment of aldosterone-related cardiovascular diseases.

Cytochrome P450 11B2 (CYP11B2), also known as aldosterone synthase, is predominantly expressed in the zona glomerulosa of the adrenal gland. As a member of the cytochrome P450 (CYP) superfamily, CYP11B2 plays an important role in three sequential oxidative reactions that catalyzes the synthesis of ALD^{20,21}. Moreover, it has gained greater attention as a promising target for the treatment of hyperaldosteronism-related cardiovascular diseases. FAD286 is a CYP11B2 inhibitor, however, FAD286 showed a 6-fold selectivity for inhibiting human recombinant CYP11B1 activity *versus* human recombinant CYP11B2 activity *in vitro*^{22,23}. LCI699, a second-generation CYP11B2 inhibitor, has been used to reduce blood pressure by lowering plasma ALD levels but failed to show acceptable selectivity for aldosterone *versus* cortisol inhibition in humans^{24,25}. This evidence illustrates the difficulty in developing selective inhibitors for similar enzymes.

Atractylodes macrocephala Koidz. (Baizhu) has a long history of treatment for edema²⁶. Atractylenolide-I, -II, and -III (AT-I, AT-II, and AT-III), as naturally occurring sesquiterpene lactones, were isolated from Baizhu²⁷. In our study, AT-I was found to have a significant diuretic effect by promoting Na⁺ excretion and preserving K⁺ in water-loaded mice by reducing the generation of ALD, without affecting the production of cortisol. However, the mechanism by which AT-I regulates the biosynthesis of ALD has not yet been identified.

To investigate the mechanism, chemical biology was coupled with activity analyses *in vivo* and *in vitro*, and the results show that AT-I covalently binds to CYP11B2 and inhibits ALD production.

The benefits not only provide a natural selective covalent inhibitor of CYP11B2 and reveal mechanistic insight into the diuretic activity of AT-I, but also provide a basis for the development of selective CYP11B2 inhibitors based on sesquiterpene lactones for the treatment of ALD-related diseases.

2. Materials and methods

2.1. Chemicals and reagents

AT-I (purity > 98%), AT-II (purity > 98%), AT-III (purity > 99%), and spironolactone (Spi, purity > 98%) were purchased from Aladdin (Beijing, China). Enzyme-linked immunosorbent assay (ELISA) kits for estradiol, progesterone (Prog), cortisol (Cort), and ALD were purchased from Cloud-Clone Corp. (San Francisco, CA, USA). Corticosterone (Cor) was purchased from J&L Biological Co., Ltd. (Shanghai, China). LCI699 (purity > 98%) and angiotensin II (Ang II, purity > 98%) were obtained from MedChemExpress (Rocky Hill, NJ, USA). The mouse monoclonal CYP11B2 antibody (MABS1251) was purchased from Millipore Corporation (Billerica, MA, USA). A His-tag polyclonal antibody (YG0002) and horseradish peroxidase (HRP) × goat anti-mouse IgG (H + L) secondary antibody (RS0001) were purchased from ImmunoWay Biotechnology Company (Plano, TX, USA). Antibodies against β -actin (#4970) and goat anti-rabbit IgG secondary antibodies (#98164) were purchased from Cell Signaling Technology (Beverly, MA, USA). Alexa Fluor® 594-conjugated goat anti-mouse IgG (ab150116) was purchased from Abcam (Cambridge, UK). Bodipy TMR azide (BDP) was purchased from Aladdin. The azido-coumarin probe was delegated to Wuxi AppTec (Beijing, China). Tris-(2-carboxyethyl) phosphine hydrochloride (TCEP) was purchased from Meilunbio® (Dalian, China), and 4% paraformaldehyde, glutathione (GSH), dithiothreitol, tris-(benzyltriazolylmethyl) amine (TBTA), dimethyl sulfoxide (DMSO), and the ethylene diamine tetraacetic acid (EDTA) were purchased from Beijing Solarbio Science & Technology Co., Ltd. (Beijing, China).

2.2. Cell culture

The human adrenocortical carcinoma cell line (NCI-H295R) was purchased from the American Type Culture Collection (Rockville, MD, USA) and was cultured in DMEM supplemented with 10% fetal bovine serum, 100 U/mL penicillin, and 100 μ g/mL streptomycin at 37 °C and 5% CO₂ in a humidified incubator.

2.3. Animals

Male C57BL/6J mice (4 weeks, 18–22 g) were purchased from the Beijing Vital River Laboratory Animal Technology Co., Ltd. (Beijing, China). The animals were randomly assigned to cages and allowed free access to water and standard mouse chow under controlled temperature (25 °C) and humidity with a 12:12-h light–dark cycle. All animal experiments were carried out in accordance with the National Institutes of Health Guide for the Care and Use of Laboratory Animals and were approved by the Tianjin University of Traditional Chinese Medicine of Laboratory Animals Care and Use Committee (TCM-LAEC2019013; Tianjin, China).

2.4. Diuretic effect in water-loaded mice

Male mice were randomly assigned to three groups ($n = 6$ in each group): (1) the control group (Con, i.p. saline), (2) the Spi group (i.p. 20 mg/kg/day spironolactone for 1 week), and (3) the AT-I group (i.p. 20 mg/kg/day AT-I for 1 week). All injections were prepared in normal saline containing 4% Tween-80. Mice were acclimated for 1 day in metabolic cages (Tecniplast Labware) and their urinary bladders were emptied by gentle compression of the pelvic area and pulling their tails before diuretic testing. Each mouse was intragastrically administered 100 mL/kg normal saline to impose a uniform water load. The 24 h urine was collected and the Na^+ and K^+ content was measured using commercial kit assays (Nanjing Jiancheng Technology, Nanjing, China). After 24 h of administration, the serum was harvested for Prog, Cort, Cor, and ALD analyses.

2.5. Aldosterone production analysis in NCI-H295R cells

NCI-H295R cells were cultured in 96-well plates, followed by serum starvation for 24 h. The culture supernatants were then replaced with medium containing vehicle (0.1% DMSO) and AT-I, AT-II, or AT-III (0.1–100 $\mu\text{mol/L}$) with or without Ang II (50 nmol/L). After 24 h of incubation, the concentrations of Prog, Cort, Cor, and ALD in the culture supernatants were measured using ELISA kits according to the manufacturer's instructions.

2.6. Cellular thermal shift assay (CETSA)

CETSA was used to detect stability changes in the CYP11B2 protein, according to a previously reported method^{28,29}. The method is summarized as follows: NCI-H295R cell lysates were treated with AT-I, AT-II, or AT-III (10 $\mu\text{mol/L}$) for 12 h at different temperatures (37, 40, 43, 46, 49, 52, 55, 58, and 61 °C) or treated with different concentrations of AT-I (0.01, 0.1, 1, 2.5, 5, 10, 20, and 50 $\mu\text{mol/L}$) for 12 h at 55 °C, and Western blot was used to determine the change in CYP11B2 protein.

2.7. Western blot

Proteins were separated by 10% sodium dodecyl sulfate-polyacrylamide gel electrophoresis (SDS-PAGE) and electrotransferred to polyvinylidene fluoride membranes. The membranes were incubated in mouse monoclonal CYP11B2 antibody (1:1000) overnight at 4 °C and incubated in the anti-mouse secondary antibody (1:5000) at 15–25 °C for 2 h. Immunoreactive bands were detected by incubation with chemiluminescent HRP substrates and exposed in a FluorChem E imager (ProteinSimple, Santa Clara, CA, USA). The density of protein was determined using the Quantity One software and normalized to their respective controls.

2.8. Target fishing and co-localization

An alkynyl-AT-I probe (AAT-I) was synthesized and used to build AAT-I-functionalized magnetic microspheres (AAT-I-beads) for target fishing in living cells or tissue. The synthesis process and identification results of AAT-I are detailed in [Supporting Information Figs. S1–S5](#).

NCI-H295R cells were incubated with 1 $\mu\text{mol/L}$ AAT-I probe for 12 h at 37 °C and cells were washed with phosphate-buffered saline prior to cell lysis. Cell lysates were then treated with azide

microspheres in click buffer (1 $\mu\text{mol/L}$ CuSO_4 , 1 $\mu\text{mol/L}$ TCEP, and 0.1 $\mu\text{mol/L}$ TBTA in 10% DMSO) for 12 h at 4 °C. AAT-I-labeled proteins were enriched by the magnetic force of the microspheres. Upon AAT-I-bead enrichment, samples were reduced with 100 mmol/L dithiothreitol (30 min at 25 °C). The target protein was analyzed by Coomassie brilliant blue staining and Western blot. The schematic diagram of target capture and identification in cells is shown in [Supporting Information Fig. S6](#).

The co-localization of target protein and AT-I in cells was verified according to a previously reported method³⁰. The click product of coumarin-AAT-I showed a strong fluorescence, while the two substrates (azido coumarin and AAT-I probe) showed almost no fluorescence ([Supporting Information Fig. S7](#)). The NCI-H295R cells were treated with 1 or 10 $\mu\text{mol/L}$ AT-I, 1 $\mu\text{mol/L}$ AAT-I probe for 6 h and then fixed with 4% paraformaldehyde. The fixed cells were incubated with azido-coumarin tracer in click buffer (1 $\mu\text{mol/L}$ CuSO_4 , 1 $\mu\text{mol/L}$ TCEP, and 0.1 $\mu\text{mol/L}$ TBTA in 10% DMSO) for 2 h at 37 °C. Then, the cells were incubated with the CYP11B2 antibody (1:500) at 4 °C overnight and with Alexa Fluor® 594-conjugated goat anti-mouse antibody (1:1000) for 30 min at 37 °C. Fluorescence imaging was performed using a laser-scanning confocal microscope Leica SP8 (Carl Zeiss, Oberkochen, Germany). Detection of the AAT-I probe was at 488/516 nm (Ex/Em), and CYP11B2 was at 594/617 nm (Ex/Em).

To capture and trace the targets in tissue, the adrenal tissue lysate or section of mice which were administered AT-I (i.p. 20 mg/kg/day) or AAT-I (i.p. 20 mg/kg/day) for one week was incubated with azide-functionalized beads or azido-coumarin tracer in the same way as described above. Pearson's correlation coefficient (PCC) was determined using the ImageJ software (National Institutes of Health, USA).

2.9. Transient transfection with CYP11B2 small interfering RNA (siRNA)

NCI-H295R cells were transfected with CYP11B2 siRNA or control negative siRNA (Santa Cruz Biotechnology, Inc. Santa Cruz, CA, USA) using Lipofectamine 3000 Transfection Reagent (Invitrogen, Carlsbad, CA, USA) for 48 h. The transfected cells were used to evaluate the production of ALD.

2.10. Identification of AT-I/GSH conjugate by UPLC/Q-TOF-MS

NCI-H295R cells were treated with 1 mmol/L GSH (GSH group), 1 mmol/L GSH and 50 $\mu\text{mol/L}$ AT-I (GSH + AT-I group), 1 mmol/L EDTA, 1 mmol/L GSH, and 50 $\mu\text{mol/L}$ AT-I (EDTA + GSH + AT-I group), respectively. After 24 h of administration, the cell lysate was treated with 3 times the volume of methanol to remove the protein. After centrifugation, the supernatant was harvested for ultra-performance liquid chromatography/quadrupole-time-of-flight-mass spectrometry (UPLC/Q-TOF-MS) analysis. The details are listed in the supplementary information.

2.11. Expression and purification of human CYP11B

The mitochondrial targeting peptide of CYP11B was removed and a MATKAAR peptide was added to the 26th residue of the N-terminal of CYP11B1 and to the 30th residue of CYP11B2, and a His \times 6 tag was added at the C-terminal. The cDNAs of human CYP11B1 and CYP11B2 were cloned into pET-17b vector and delegated to BGI Technology Co., Ltd. (Beijing, China). The

recombinant wild-type human CYP11B2 protein (WT), recombinant Ala320 mutant CYP11B2 protein (A320V, Ala mutated to Val), Cys450 mutant CYP11B2 protein (C450G, Cys mutated to Gly), and recombinant wild-type human CYP11B1 protein were co-expressed with GroEL/ES in *E. coli*. Expression was induced by the addition of 0.5 mmol/L isopropyl-1-thio-D-galactopyranoside, 4 mg/mL arabinose, and 1 mmol/L δ -aminolevulinic acid heme precursor, and the culture was incubated another 48 h at 26 °C. Purification was performed as previously described³¹. The detailed protein expression and purification procedures are shown in [Supporting Information Fig. S8](#).

The specificity of CYP11B2 antibody was verified by using the recombinant human CYP11B1 and CYP11B2 as shown in [Supporting Information Fig. S9](#).

2.12. In-gel imaging

To evaluate the irreversible binding of AT-I to CYP11B2, the AAT-I-labeled protein was illuminated by the BDP TMR azide fluorophore in the gel. In the post-incubation group, recombinant CYP11B2 protein was pre-incubated with 100 μ mol/L AAT-I at 4 °C for 12 h, and was further incubated with 0–100 μ mol/L AT-I (or its derivatives AT-II and AT-III) for 12 h for competitive binding. In the co-incubation group, recombinant CYP11B2 protein was co-incubated with 100 μ mol/L AAT-I and 0–100 μ mol/L AT-I. Both groups were added to the NCI-H295R cell lysates (0.1 mg/mL) as the enzymatic reaction solution. The samples were incubated with the click reaction solution (10 μ mol/L BDP TMR azide, 1 μ mol/L CuSO₄, 1 μ mol/L TCEP, and 0.1 μ mol/L TBTA in distilled water) for 1 h at 37 °C to produce a fluorescent indicator. The unbound fluorophore tracer was removed by washing with MeOH and centrifugation. Sodium dodecyl sulfate (0.5%) in phosphate-buffered saline was added for 5 min at 65 °C to dissolve the pelleted protein and the supernatants were collected for SDS-PAGE. For in-gel fluorescence imaging, the gels were scanned on a Tanon-5200 Multi Gel Imaging System (Tanon 8 Science & Technology, Shanghai, China) for the BDP-AAT-I-labeled protein assay. As a control, the gel was transferred to polyvinylidene fluoride membranes for Western blot analysis.

For in-gel imaging of mouse adrenal glands, the mice were treated continuously with AT-I (i.p. 20 mg/kg/day) or AAT-I (i.p. 20 mg/kg/day) for one week. Then, adrenal gland lysates were collected and the click reaction was carried out as described above.

2.13. Carbon monoxide (CO) difference spectra

After the reduced P450 enzyme binds to CO, the protein has a significant absorption peak at about 450 nm³². Hence, the effect of atracylodes lactone on the binding of heme to CYP11B was detected by CO difference spectra. Recombinant CYP11B1 or CYP11B2 (0.1 mg/mL) was incubated with AT-I, AT-II, or AT-III (10 μ mol/L) in 50 mmol/L potassium phosphate buffer, pH 7.4 (containing 150 mmol/L NaCl and 20% glycerol) for 12 h at 4 °C. The sample was reduced with sodium dithionite and exposed to 100% CO for 3 min in an airtight container. Subsequently, the reduced CO complex was scanned to record the CO difference spectra between 400 and 780 nm with 2 nm interval by an Evolution™ 200 UV–Visible spectrophotometer (Thermo Fisher Scientific, Inc., Waltham, MA, USA).

2.14. Fluorescence-based thermal shift (FTS) assay

The recombinant human CYP11B1, CYP11B2, or mutant protein C450G of CYP11B2 was incubated with NCI-H295R cell lysates (0.1 mg/mL) and AT-I or its derivatives (AT-II and AT-III, 20 μ mol/L) for 12 h at 4 °C. The separated CYP11B protein was incubated with the Protein Thermal Shift Dye Kit TM (1:6000) in a total volume of 20 μ L in a 96-well plate. Scanning (37–95 °C at 0.03 °C/s) was conducted using a real-time PCR machine (Light Cycler 96, Roche, Switzerland). Data collection and analysis of the thermal stability were consistent with those reported in the literature³³.

2.15. Molecular docking

The three-dimensional structures of the CYP11B2 protein (PDB: 4FDH) were obtained from the Protein Data Bank (<http://www.rcsb.org/pdb>). The structures of the C8/C9 epoxy AT-I and CYP11B2 proteins were constructed and minimized using SYBYL software (Chemical Computing Group, Inc., Cambridge, UK), and Schrödinger_2018 software (Schrödinger, Inc., New York, NY, USA) was used for covalent docking. The nucleophilic receptor was set as all cysteine in the protein, and the reaction type was set as the epoxide opening reaction. The binding mode and reaction site was analyzed using Pymol software (Schrödinger, Inc., New York, NY, USA).

2.16. Surface plasmon resonance (SPR) assay

The interaction between recombinant human CYP11B2 and mutant protein A320V of CYP11B2 with AT-I and AT-II was performed using a Biacore T200 optical biosensor (GE Healthcare, Pittsburgh, PA, USA). The proteins were immobilized on a CM5 chip. During each binding cycle, AT-I or AT-II solution (3.9–500 μ mol/L) was injected at a flow rate of 10 μ L/min for 1 min, and the dissociation was monitored for 300 s. Data collection and analysis was as described in the literature^{34,35}.

2.17. Ang II-induced hyperaldosteronism test in mice

Male mice were randomly divided into 6 groups ($n = 10$ in each group), and each group was treated in the following manner: control (Con, i.p. saline), model (Mod, i.p. Ang II, 4 mg/kg/day), AT-I-H (i.p. Ang II + AT-I 40 mg/kg/day), AT-I-M (i.p. Ang II + AT-I 20 mg/kg/day), AT-I-L (i.p. Ang II + AT-I 10 mg/kg/day), and Spi (i.p. Ang II + Spi 20 mg/kg/day). All injections were prepared in normal saline containing 4% Tween-80. All groups received injections for 7 days and the last day's urine was collected from each mouse using a metabolic cage. The urine and serum were harvested for Na⁺, K⁺, Cl⁻, estradiol, Cort, and ALD analyses. Heart rate (HR), systolic blood pressure (SBP), diastolic blood pressure (DBP), and mean blood pressure (MBP) were measured by a computerized mouse tail-cuff system (BP-98A, Softron Corp., Tokyo, Japan) before and at the 7th day of the Ang II infusion. The basal HR, SBP, DBP, and MBP of each group were similar before Ang II stimulation ([Supporting Information Fig. S10](#)).

2.18. Statistical analysis

Each experiment consisted of at least three replicates per condition. All data are expressed as mean \pm SD. Data were analyzed by

an unpaired *t*-test or one-way ANOVA followed by Dunnett's *post hoc* test using GraphPad InStat (version 5.0; GraphPad Software, Inc., San Diego, CA, USA). $P < 0.05$ was considered statistically significant.

3. Results

3.1. AT-I causes diuresis by reducing serum ALD

ALD is the most important mineralocorticoid involved in the regulation of body fluids and the exchange of Na^+ and K^+ . As shown in Fig. 1A–C, AT-I has a significant diuretic effect of increasing Na^+ excretion and decreasing K^+ loss. AT-I significantly reduced the serum ALD content, but it did not affect Prog and Cort levels (Fig. 1D–F). ALD is synthesized from cholesterol in the zona glomerulosa of the adrenal gland through a cascade of steroid hydroxylases and dehydrogenase³⁶. The synthesis of Cort and ALD is shown in Fig. 1G; CYP11A1 utilizes cholesterol for the formation of pregnenolone, and CYP17 converts Prog to 17- α -OH-progesterone. Prog is also a substrate for CYP21A2 and can be converted to 11-deoxycorticosterone. CYP11B1 can catalyze 11-deoxycorticosterone or 11-deoxycortisol hydroxylation to produce corticosterone and Cort, while CYP11B2 can only catalyze 11-deoxycorticosterone oxidation to produce corticosterone and further hydroxylation to ALD. In water-loaded mice, AT-I also significantly reduced the content of serum corticosterone, as shown in Supporting Information Fig. S11.

This result suggests that AT-I may inhibit ALD production by acting in the final three steps of ALD biosynthesis. The final three steps of ALD biosynthesis are catalyzed by CYP11B2. Therefore, we speculated that AT-I may inhibit ALD production by acting on CYP11B2.

3.2. AT-I interacts with CYP11B2 to inhibit the generation of ALD

To explore the selectivity of AT-I, the effects of different types of atractyloides lactones on ALD production were evaluated in NCI-H295R cells. The chemical structures of AT-I, AT-II, and AT-III are shown in Fig. 2A. The test results showed that AT-I significantly inhibited Cor and ALD generation, while it had no significant influence on the intermediate products Prog and Cort; AT-III inhibited the production of Cort, Cor, and ALD; however, AT-II had very little ability to suppress Prog, Cort, and ALD production (Fig. 2B–E).

The potential interaction capacities of AT-I and its derivatives to CYP11B2 were investigated using CETSA. As shown in Fig. 2F, it was found that AT-I treatment efficiently altered the thermal stability of CYP11B2, but AT-II and AT-III did not affect the thermal stability of CYP11B2. The inhibitory effect of AT-I was dose-dependent at 55 °C, and the half maximal inhibitory concentration (IC_{50}) was about 8.0 $\mu\text{mol/L}$ (Fig. 2G). In addition, AT-I was also demonstrated to inhibit the generation of ALD in NCI-H295R cells, but with little cytotoxicity, which was tested using the Cell Counting Kit-8 reagent (MedChemExpress, Rocky Hill, NJ, USA). The IC_{50} value was 7.7 $\mu\text{mol/L}$, which was consistent with the result of CETSA (Fig. 2H). The structure–activity analysis suggested that the binding capacity of CYP11B2 and AT-I was related to the double bond of AT-I at the C8/C9 site.

3.3. CYP11B2 is a potential target of AT-I

To verify the binding between CYP11B2 and AT-I, different AT-I probes were prepared for target protein capture and fluorescent labeling (Fig. 3A). The AAT-I probe was used to pull down the cellular target of AT-I by forming functional magnetic spheres (AAT-I bead) with a [3+2] cycloaddition reaction. The AAT-I probe also could be conjugated with azido-coumarin as a fluorescent tracer used for fluorescence imaging in NCI-H295R cells. Fortunately, the modified AAT-I probe, with a new alkynyl group introduced at the C3 position, was also able to lower ALD release as effectively as the original compound (Fig. 3B).

As presented in Fig. 3C, an obvious protein band could be noted between 50 and 60 kDa in the pull-down group with AAT-I beads; however, the band was barely detectable in the control beads group. Western blot also verified this protein with a specific anti-CYP11B2 antibody. To verify this result, a co-localization test between the CYP11B2 protein and the AAT-I probe was carried out with NCI-H295R cells. As shown in Fig. 3D, pseudo-green fluorescence was observed in the coumarin-AAT-I group, while the control and AT-I groups showed little pseudo-green fluorescence. Notably, the specific fluorescence of the CYP11B2 antibody (pseudo-red) partially merged with the AAT-I probe (pseudo-green, $\text{PCC} = 0.782$). Moreover, this phenomenon could be competitively inhibited by the addition of a 10-fold excess of AT-I.

To confirm whether AT-I inhibits the generation of ALD by acting on CYP11B2, an RNA interference test was carried out, which transiently knocked down *CYP11B2* in NCI-H295R cells (Fig. 3E). As shown in Fig. 3F, the knockdown of *CYP11B2* completely abolished the AT-I-mediated inhibition of ALD production. LCI699, an existing inhibitor of CYP11B2, also no longer showed a significant inhibitory effect on ALD production. However, a further study found that AT-I did not change the protein expression level of CYP11B2 in NCI-H295R cells at different doses and incubation times (Supporting Information Fig. S12). The above results indicated that AT-I might directly target CYP11B2 and inhibit its enzymatic activity for ALD production.

3.4. AT-I covalently binds to CYP11B2 via an epoxidation process

CYP enzymes, also known as monooxygenases, can catalyze the epoxidation of a C–C double bond with the heme iron cofactor as an auxiliary group^{37,38}. To reveal the binding mode between AT-I and CYP11B2, AT-I was incubated with GSH in NCI-H295R cells and the reaction products were detected by UPLC/Q-TOF-MS. As shown in Fig. 4A, a major nucleophilic addition product, [AT-I+O+GSH] m/z 554.21, was indicated. At the same time, an extra intermediate peak of epoxidized AT-I, [AT-I+O] m/z 247.13, was also detected. After adding EDTA to chelate Fe^{3+} ions, the peaks were weakened. However, AT-II did not react with GSH to form a mass spectrum peak, nor did it form an epoxidized AT-II peak (Supporting Information Fig. S13). These results suggest that the C8/C9 double bond of AT-I may be first epoxidized by the intracellular P450 enzyme and then react with the sulfhydryl group of GSH.

As a member of the CYP superfamily, CYP11B plays an important role in catalytic hydroxylation and oxidation of substrates. Therefore, we further verified whether AT-I can be epoxidized by recombinant CYP11B proteins. The results of UPLC/Q-

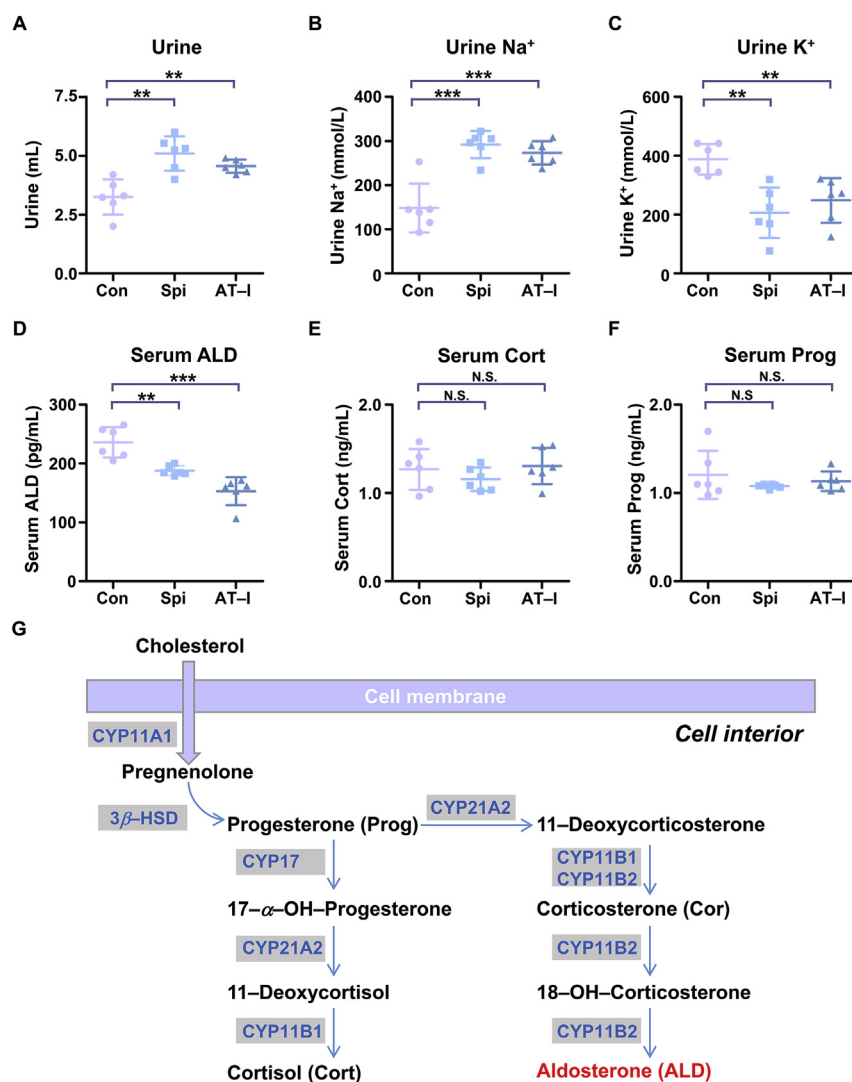


Figure 1 The diuretic effect of AT-I in water-loaded mice. (A) The effects of AT-I on the urine volume of mice. (B) and (C) The effects of AT-I on the content of urine Na⁺ and K⁺ in mice. (D)–(F) The effects of AT-I on the content of serum ALD, Cort, and Prog of mice. After received physiological solution alone (Con) or solution containing 20 mg/kg/day spironolactone (Spi) or 20 mg/kg/day AT-I (AT-I) for one week, the mice were given an oral dose of physiological solution (0.9% NaCl, 100 mL/kg body weight) to impose a uniform water and salt state ($n = 6$). Data are expressed as means \pm SD. ** $P < 0.01$, *** $P < 0.001$ vs. Con; N.S., no statistical difference. (G) The synthesis pathway of cortisol and aldosterone.

TOF-MS identification showed that the CYP11B2 could catalyze the epoxidation peak of AT-I, while CYP11B1 could not (Fig. 4B). To test whether AT-I could covalently bind to CYP11B2, an in-gel fluorescent imaging assay was performed. As shown in Fig. 4C, a specific fluorescent band at approximately 58 kDa for BDP-AAT-I-labeled CYP11B2 protein was detected, but the CYP11B1 protein could not be labeled by BDP-AAT-I. The fluorescence intensity of BDP-AAT-I-labeled CYP11B2 protein was attenuated by co-incubation with AT-I. However, when CYP11B2 was pre-incubated with the AAT-I probe, post-treatment with an excess amount of AT-I could not prevent BDP-AAT-I-labeled CYP11B2 protein (Fig. 4D). Taken together, the evidence suggests that AT-I could be specifically epoxidized and then covalently bound to CYP11B2.

3.5. AT-I selectively targets CYP11B2 based on the C8/C9 double bond of AT-I

To further explore the structure–activity relationship of AT-I, AT-II, and AT-III were introduced to test the interaction between drug and CYP11B proteins. As shown in Fig. 5A, the in-gel imaging result shows that the BDP-AAT-I-labeled CYP11B2 band was significantly decreased by pre-incubation with an excess amount of AT-I, but not AT-II and AT-III. This suggests that the C8/C9 double bond may be the key pharmacophore in the structure of AT-I for binding to CYP11B2. To verify the significance of the C8/C9 double bond, a CO difference spectroscopy assay was performed. As shown in Fig. 5B, there was a typical absorption peak of reduced CYP11B2–CO complex at 450 nm, but only AT-I showed

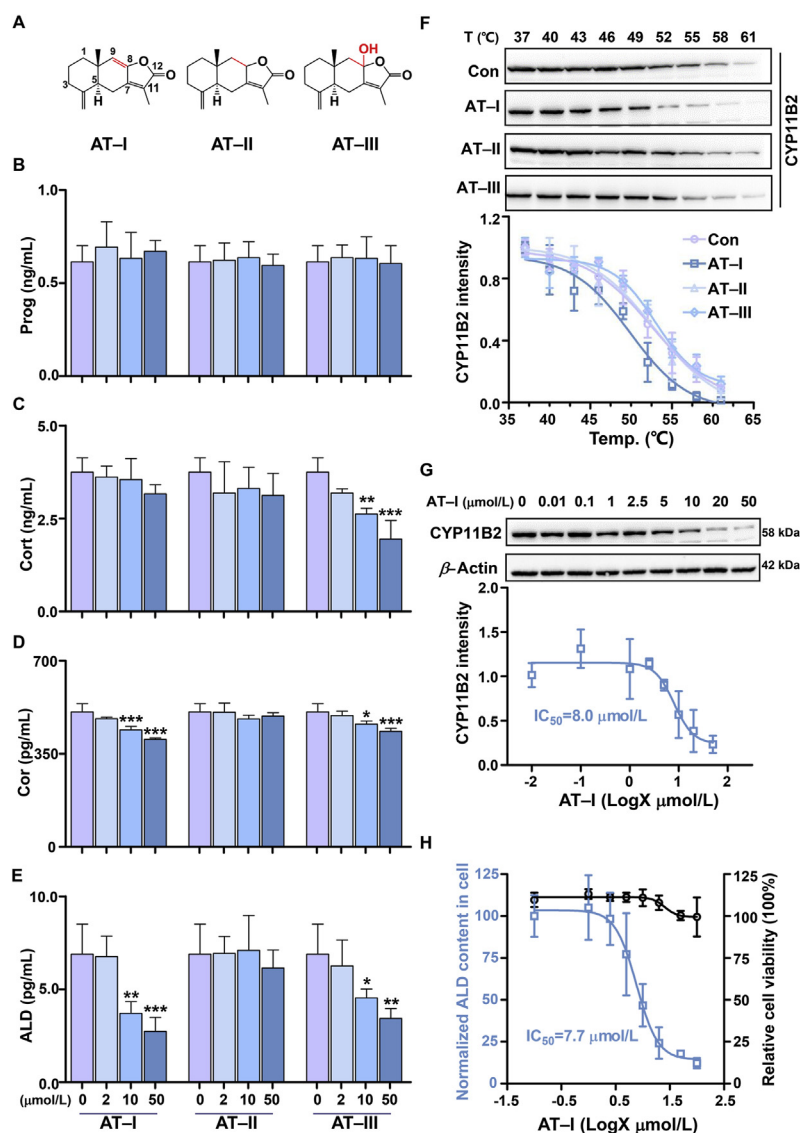


Figure 2 AT-I inhibits the production of ALD in NCI-H295R cells by interacting with CYP11B2. (A) The chemical structure of AT-I, AT-II, and AT-III. (B)–(E) Inhibitory effect of AT-I and its derivatives on Prog, Cort, Cor, and ALD production. NCI-H295R cells were treated with different concentrations of AT-I and its derivatives (AT-II and AT-III) for 24 h, then Prog, Cort, Cor, and ALD were measured ($n = 4$). (F) AT-I/II/III treatment (10 $\mu\text{mol/L}$) influences the thermal stability of CYP11B2 as assayed by CETSA ($n = 3$). (G) AT-I treatment reduces the thermal stability of CYP11B2 in a dose-dependent manner at 55 $^{\circ}\text{C}$ ($n = 3$). (H) Evaluation of ALD-inhibiting effects and cell viability of AT-I treatment in NCI-H295R cells ($n = 4$). Data are expressed as means \pm SD. * $P < 0.05$, ** $P < 0.01$, *** $P < 0.001$ vs. Con group that was not drug-treated.

the ability to affect the structural integrity of the CYP11B2 protein. It is worth noting that neither AT-I nor its derivatives affect the formation of the reduced CYP11B1–CO complex (Fig. 5C). In addition, we also verified the effect of AT-I derivatives on the thermal stability of CYP11B1 protein. As shown in Fig. 5D, AT-III weakened the thermal stability of CYP11B1, while AT-I and AT-II had no effect. This result indicates that the hydroxyl group at the C8 position of AT-III might play a key role in the selectivity of CYP11B1. Overall, the results demonstrate that AT-I is a selective, covalent inhibitor of CYP11B2 but not CYP11B1, and its inhibitory activity mainly relies on the epoxidation of a specific double-bond group at the C8/C9 site of AT-I.

3.6. AT-I inhibits CYP11B2 by relying on both Cys450 and Ala320 of CYP11B2

To clarify the mechanism of selective catalysis, the interaction between AT-I and CYP11B2 was simulated by molecular docking (Fig. 6A). The covalent docking results show that a strong interaction is only evident between the epoxidized AT-I and Cys450 amino acids of CYP11B2. It has been reported that the Ala320 of CYP11B2 plays a key role in the 18-oxidation activity of the enzyme, and the Ala320 active site at CYP11B2 leads to the selectivity of CYP11B2 and CYP11B1 to catalyze different substrates^{39–41}. Sequence comparison, as shown in Fig. 6B, indicates

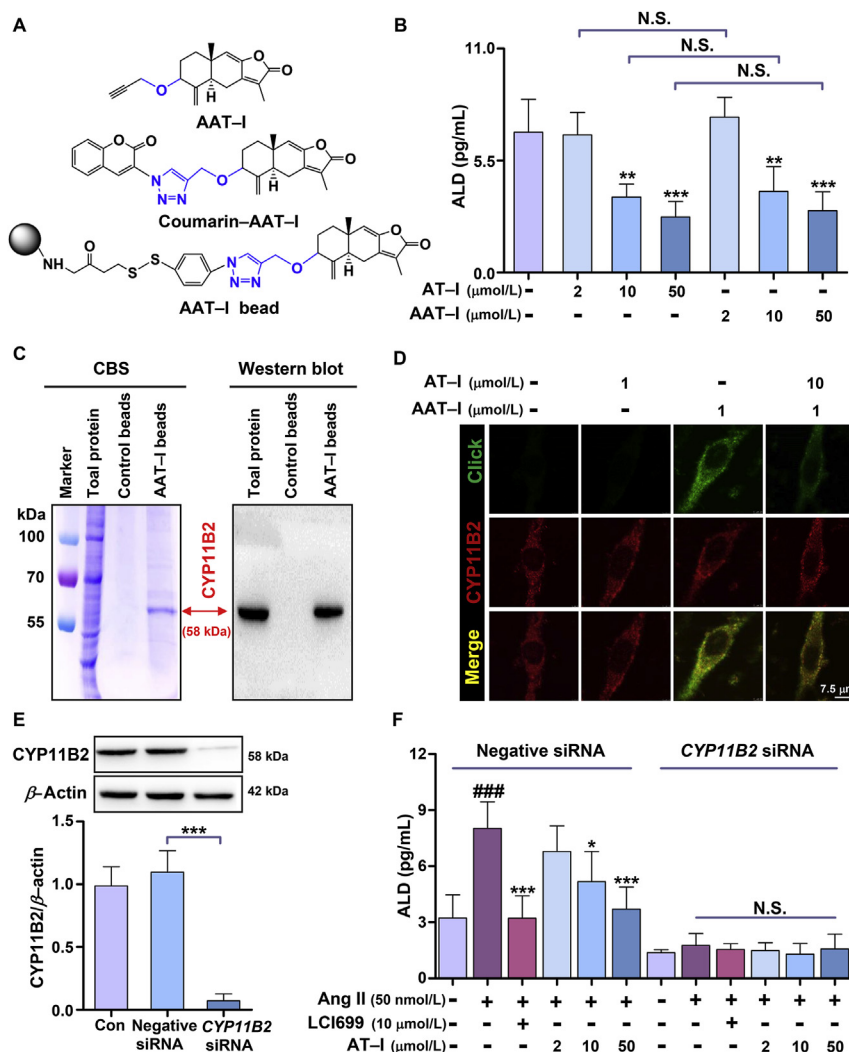


Figure 3 AAT-I molecular probes and siRNA interference test reveal that CYP11B2 is the target of AT-I. (A) The chemical structure of the AAT-I probe and its derivative coumarin-AAT-I fluorescent tracer and AAT-I bead formed by clicking reaction. (B) The ALD release assay with AAT-I probe or AT-I treatment in NCI-H295R cells ($n = 4$). (C) Fishing and identifying the potential target protein CYP11B2. Coomassie brilliant blue stain (CBS, left panel) and Western blot analysis (right panel) were used to detect the protein CYP11B2 enriched by AAT-I beads. The marker shows the molecular weight. (D) The co-localization imaging of CYP11B2 protein and AAT-I in NCI-H295R cells with fluorescent confocal microscopy. The AAT-I probe took on a pseudo-green color *via* the click reaction, and the pseudo-red color represents CYP11B2, which was stained by Alexa Fluor® 594. The yellow merger represents CYP11B2 colocalized with AAT-I. Cells were treated with 1 or 10 μmol/L AT-I, 1 μmol/L AAT-I for 6 h. Scale bar: 7.5 μm. (E) The prevention of CYP11B2 protein expression using a specific *CYP11B2* siRNA. Western blot analysis was performed after transfection of NCI-H295R cells with *CYP11B2* siRNA for 48 h ($n = 3$). (F) ALD release assay of AT-I treatment in NCI-H295R cells, which was induced by Ang II in the absence or presence of *CYP11B2* siRNA-transfection ($n = 4$). All data are expressed as means \pm SD. ### $P < 0.001$ vs. Con; * $P < 0.05$, ** $P < 0.01$, *** $P < 0.001$ vs. Mod; N.S., no statistical difference.

that the amino acids Cys450 and Ala320 in CYP11B2 are conserved in human and mice, but differ between CYP11B1 and CYP11B2 at 320 amino acids. Therefore, we speculate that the Ala320 and Cys450 of CYP11B2 may be related to AT-I selectively targeting CYP11B2.

In support of the in-gel imaging assay results, when Ala320 in CYP11B2 was mutated to valine (A320V) or Cys450 was mutated to glycine (C450G), the mutated proteins could not be labeled by BDP-AAT-I (Fig. 6C). SPR analysis also revealed that the binding affinity of AT-I to CYP11B2 was 13.8 μmol (Fig. 6D), lower than that of the A320V mutant protein (755 μmol, Fig. 6E). It is worth noting that AT-II did not bind to either the recombinant wild-type

human CYP11B2 protein (WT) or the mutant protein A320V (Supporting Information Fig. S14). Moreover, UPLC/Q-TOF-MS showed that the WT could catalyze the epoxidation of AT-I, but the A320V mutation was observably weakened (Supporting Information Fig. S15), which suggested that the presence of Ala320 in CYP11B2 might play a key role for oxidation of the C8/C9 double bond in AT-I. Strikingly, the FTS results also support that AT-I decreases the thermal stability of CYP11B2, but does not affect the C450G mutant protein (Fig. 6F). In the CYP11B2 structure, the absolutely conserved Cys450 is liganded with the heme, so the weakened binding of heme to CYP11B2 will be a prerequisite for the binding of AT-I to Cys450. In our study, we

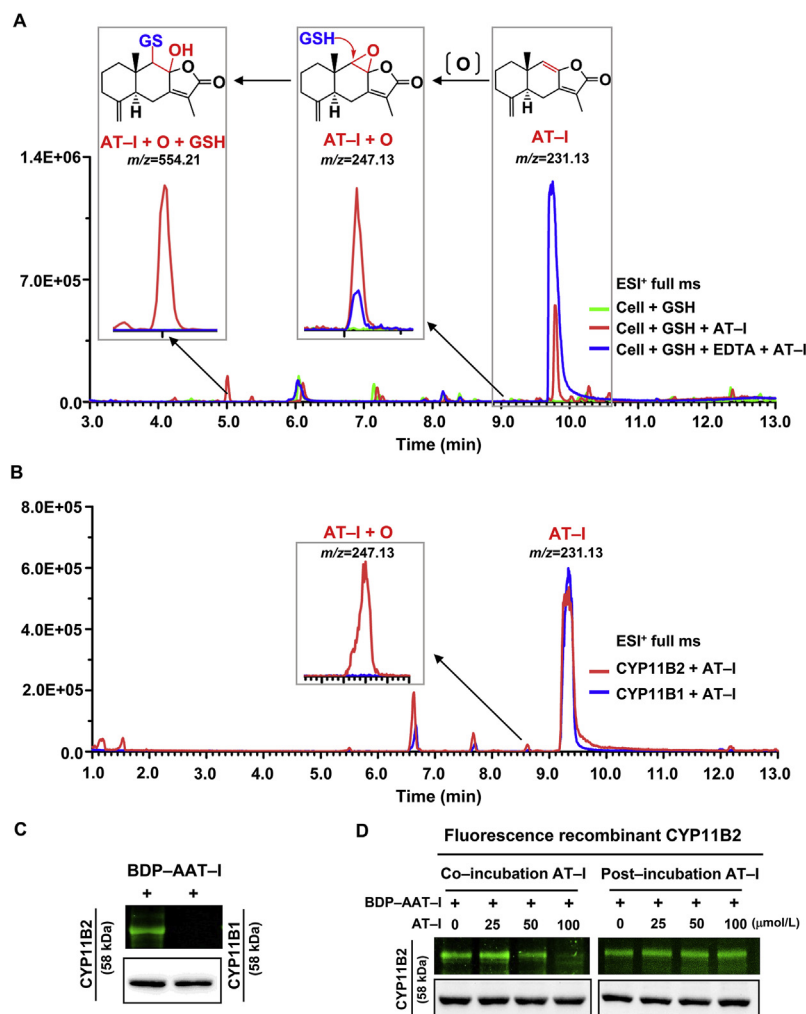


Figure 4 AT-I covalently binds with CYP11B2 *via* an epoxidation nucleophilic addition. (A) UPLC/Q-TOF-MS analysis of the incubation product of AT-I and GSH in NCI-H295R cells. NCI-H295R cells were treated with 1 mmol/L GSH or EDTA, 50 μmol/L AT-I for 24 h, and then cells were harvested for LC-MS analysis. (B) UPLC/Q-TOF-MS identification of the incubation product of AT-I and CYP11B2 or CYP11B1. (C) In-gel imaging assay of CYP11B2 or CYP11B1. (D) Irreversible binding of AAT-I to CYP11B2. In the co-incubation AT-I group, the recombinant CYP11B2 protein was incubated for 12 h with AAT-I in the absence or presence of AT-I for competitive binding. In the post-incubation group, the recombinant CYP11B2 protein was preincubated with AAT-I for 12 h and then incubated with or without AT-I for 12 h for competitive binding.

confirmed by CO difference spectroscopy that AT-I can disrupt the binding of heme to CYP11B2 in a concentration-dependent manner (Fig. 6G). In conclusion, we confirmed that Ala320 allows AT-I to enter the catalytic pocket of CYP11B2, the C8/C9 double bond of AT-I was epoxidized under the catalysis of Fe³⁺ in heme, and epoxidized AT-I bound with the Cys450 of CYP11B2. Although CYP11B1 and CYP11B2 are highly similar, AT-I cannot bind to CYP11B1 due to the lack of Ala320 in CYP11B1, so AT-I shows selectivity for CYP11B2.

3.7. AT-I alleviates Ang II-induced aldosteronism in mice by targeting CYP11B2

In order to explore the binding capacity of AT-I to CYP11B2 at the animal level, in-gel imaging analysis, target fishing, and immunofluorescence co-localization was carried out with adrenal tissue,

after the intraperitoneal injection of the AAT-I probe to mice. The in-gel imaging analysis showed that the BDP-AAT-I group exhibited a clear fluorescent band at approximately 58 kDa (Fig. 7A left panel). The magnetic fishing test confirmed that AAT-I beads could successfully capture the CYP11B2 protein from the mouse adrenal gland, and blank beads did not select the CYP11B2 protein (Fig. 7A right panel). In addition, adrenal gland tissue sections were investigated for co-localization of the CYP11B2 protein and AAT-I probe. As shown in Fig. 7B right panel, the specific pseudo-green fluorescence of the AAT-I probe was observed in the adrenal cortex. Specifically, the specific pseudo-red fluorescence of CYP11B2 was highly merged by the AAT-I probe with yellow fluorescence (PCC = 0.924), and the control and AT-I groups showed little yellow fluorescence (Fig. 7B left panel). The above evidence indicates that AT-I targets CYP11B2 in the adrenal cortex *in vivo*.

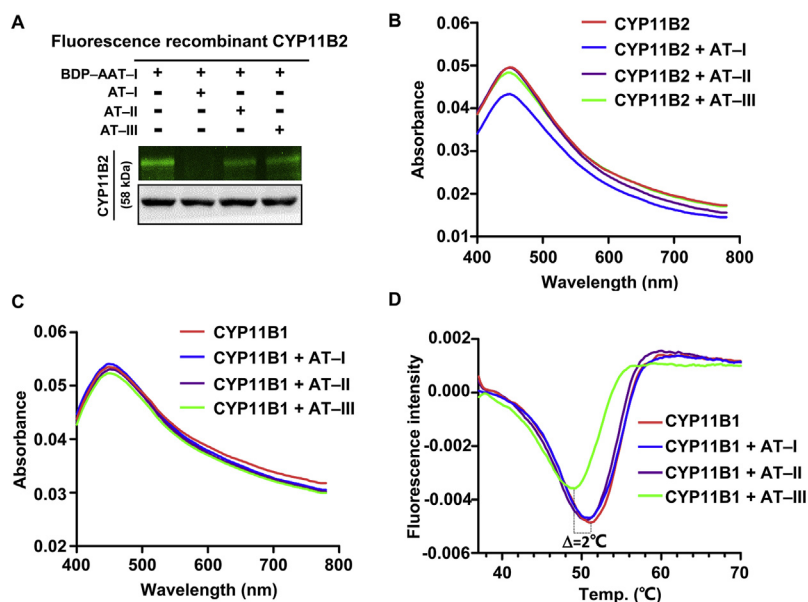


Figure 5 The C8/C9 double bond is considered to be the key pharmacophore for AT-I selective binding to CYP11B2. (A) The in-gel fluorescence competition assay of AT-I and its derivatives. Recombinant CYP11B2 proteins were incubated with AAT-I (100 $\mu\text{mol/L}$) in the absence or presence of AT-I, AT-II, or AT-III at 4 $^{\circ}\text{C}$ for 12 h, and the products were resolved by the SDS-PAGE for the in-gel imaging assay (green). (B) and (C) The CO difference spectroscopy assay of CYP11B2 or CYP11B1 for AT-I and its derivatives. Recombinant CYP11B2 or CYP11B1 protein (0.1 mg/mL) was incubated with AT-I, AT-II, and AT-III (10 $\mu\text{mol/L}$) at 4 $^{\circ}\text{C}$ for 12 h, and the products were reduced with sodium dithionite and complexed with CO. The reduced CO complex was scanned between 400 and 780 nm. (D) The FTS assay for CYP11B1 protein against AT-I, AT-II, or AT-III.

To confirm the therapeutic effect of AT-I in the Ang II-induced hyperaldosteronism model, serum and urine parameters and cardiac function were evaluated. As expected, serum Na^{+} levels were higher and serum K^{+} levels were significantly lower in the Ang II-induced hyperaldosteronism model group than in the Con group. Notably, AT-I treatment significantly reduced serum Na^{+} levels and increased serum K^{+} levels (Fig. 7C and D). Concomitantly, AT-I increased urine Na^{+} and reduced urine K^{+} induced by Ang II (Fig. 7F and G), whereas serum Cl^{-} and urine Cl^{-} levels were similar in all the groups (Fig. 7E and H). At the same time, AT-I treatment significantly reduced the levels of serum Cor (Supporting Information Fig. S16) and ALD (Fig. 7I), but did not affect the production of serum Cort (Fig. 7J) *in vivo*. In addition, we also detected changes in estrogen in this model. The results show that the content of serum estradiol in mice with hyperaldosteronism was significantly reduced, while both Spi and AT-I increased the content of serum estradiol (Fig. 7K). Aldosteronism can cause some cardiovascular dysfunction in clinical research^{8,10}. In our study, we found that the HR, SBP, DBP, and MBP of mice were significantly increased after continuous induction of Ang II, while 20 and 40 mg/kg AT-I and spironolactone treatment could significantly alleviate this phenomenon (Fig. 7L–N and Supporting Information Fig. S17).

4. Discussion

Hyperaldosteronism is associated with aldosterone synthesis and disorders of aldosterone synthesis from corticosterone^{9,42}. CYP11B2 is the terminal enzyme in the aldosterone biosynthetic pathway and is necessary for aldosterone biosynthesis. In recent years, CYP11B2 has been a promising therapeutic target for the

treatment of ALD-related cardiovascular diseases, and some CYP11B2 inhibitors appear to act as effective agents in clinical trials of hyperaldosteronism⁴³. However, due to the high similarity between CYP11B2 and CYP11B1, an enzyme that catalyzes the formation of cortisol, the current inhibitors also inhibit CYP11B1, which leads to adverse reactions and limits its clinical application⁴⁴. In the present study, we found that AT-I significantly inhibited ALD production but did not inhibit cortisol production *in vivo* or *in vitro*. This result indicates that AT-I has selectivity for CYP11B2 inhibition.

Although CYP11B1 and CYP11B2 have 93% sequence identity, there are several amino acid differences between CYP11B1 and CYP11B2 within the substrate binding site, at positions 68, V/M; 109, C/H; 112, I/S; 147, D/E; 302, E/D; 320, A/V; 404, Q/R; and 439, H/Y for CYP11B2/B1, respectively^{39–41}. These differences critically alter CYP11B1 and CYP11B2 substrate selection. CYP11B2 catalyzes the 11-hydroxylation of deoxycorticosterone to corticosterone, followed by 18-hydroxylation to produce 18-hydroxycorticosterone with further 18-oxidation of the latter to ALD. CYP11B1 also catalyzes the 11-hydroxylation of deoxycorticosterone to corticosterone, but cannot catalyze the two successive oxidations at C18 to yield the 18-hydroxy and 18-aldehyde metabolites. Ala320 is crucial for the 18-oxidase function of CYP11B2 and is important in the differential binding and orientation of the respective substrates^{39,45}. In this study, we found that AT-I could be epoxidated by the recombinant protein CYP11B2, but not by the recombinant protein CYP11B1. Notably, when Ala320 of CYP11B2 mutated to Val320, as found in CYP11B1, the ability of CYP11B2 to oxidize AT-I was diminished. This indicates that the presence of Ala320 in CYP11B2 is required for AT-I to selectively target CYP11B2 and be oxidized by CYP11B2. AT-I enters the

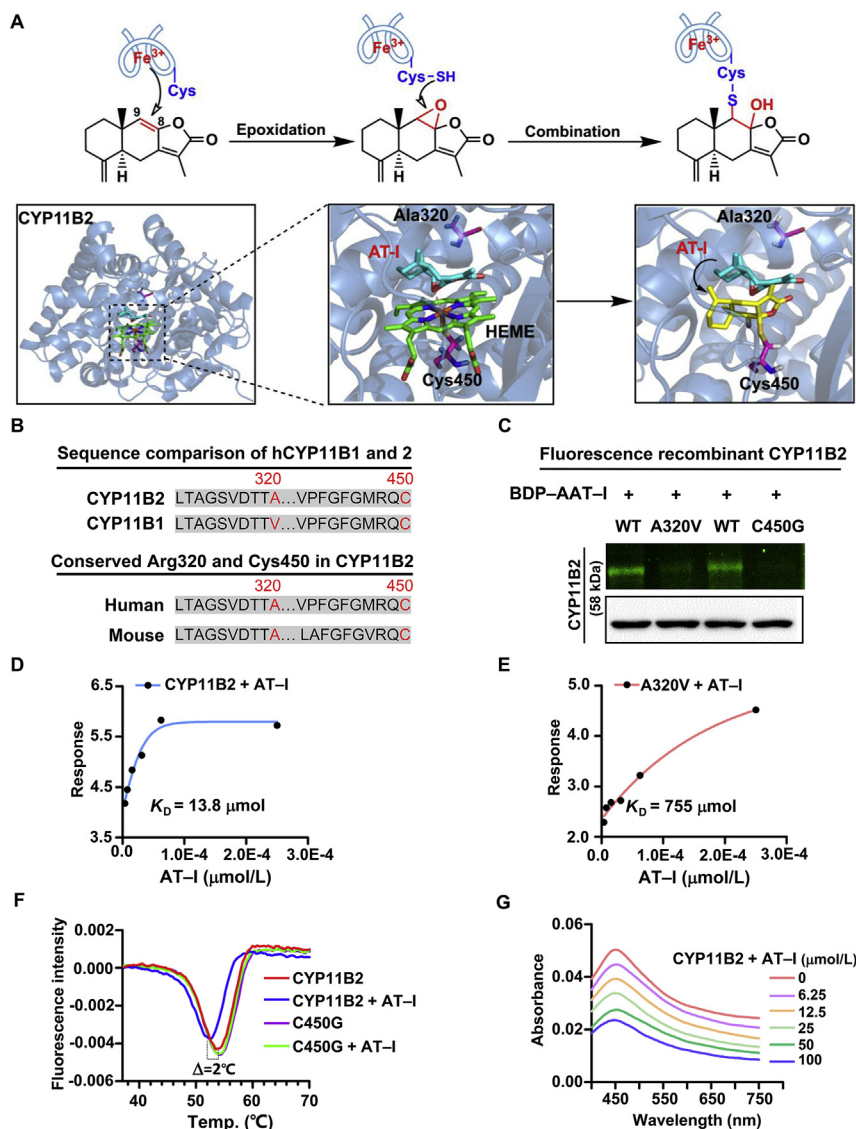


Figure 6 AT-I selectively binds with CYP11B2 relying both on Cys450 and Ala320. (A) A representative global view of AT-I with the CYP11B2 protein. Molecular modeling the 8,9 epoxy AT-I covalently bound to the Cys450 of CYP11B2. CYP11B2 protein is shown by the sky-blue ribbon model, heme is shown with the green stick model, and AT-I is shown by the cyan stick model. (B) A sequence comparison of CYP11B2 from different species and different isoforms. (C) In-gel fluorescence imaging assay for CYP11B2 (WT) protein and its mutants (A320V and C450G). (D) and (E) SPR analysis of AT-I binding to CYP11B2 or A320V. (F) The thermal shift assay of CYP11B2 or C450G protein incubated with the AT-I. (G) The CO difference spectra of CYP11B2 with AT-I.

enzyme activity pocket and is oxidized by CYP11B2, which hinders the synthesis of ALD catalyzed by CYP11B2.

Heme is an iron-porphyrin compound that is essential to CYP11B2 activity and plays a key role in the catalytic reactions of CYP11B2⁴⁶. After 11-deoxycorticosterone enters the substrate-binding pocket of CYP11B2, C11 and C18 of 11-deoxycorticosterone are placed over the heme iron, making them accessible for hydroxylation⁴⁷. The iron atom of heme is linked to the conserved Cys450 in CYP11B2, which participates in the biosynthesis of ALD⁴⁸. In this study, AT-I competitively disrupted the binding of Cys450 to heme, thereby affecting the structural stability of CYP11B2 and abolishing the production of ALD.

Epoxy compounds are important intermediates that play an important role in the fields of medicine and pharmacy. It has been

found that many natural products are effective after epoxidation through the action of CYP. For example, CYP3A4 converts carbamazepine to carbamazepine-10,11-epoxide, which is the major metabolite necessary for the anticonvulsant effect⁴⁹. Ursolic acid reduces hepatocellular apoptosis because its epoxide group covalently attaches to the thiol group of Cys163 of CASP3⁵⁰. AT-I is a sesquiterpene lactone that possesses three unsaturated double bonds. We found that AT-I with a double bond at the C8/C9 position was the key pharmacophore that could be metabolized into the intermediate epoxy product, attacking the thiol of Cys450 in CYP11B2, thus inhibiting the activity of CYP11B2. Most of the existing inhibitors of CYP11B2 are azoles or N-containing heterocyclic compounds that can competitively bind to the amino acids in the substrate pocket to prevent hydroxylation of the

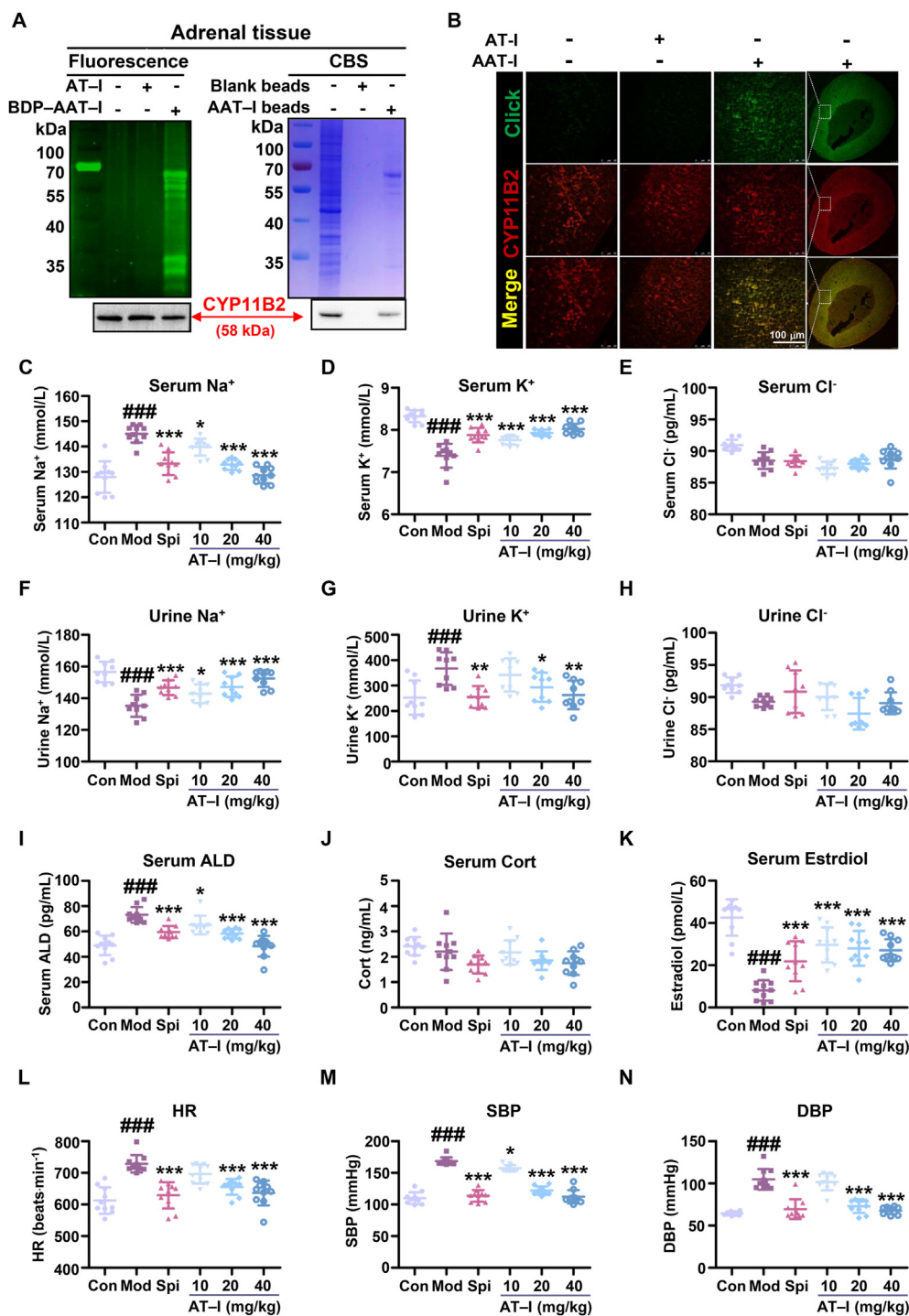


Figure 7 AT-I alleviated Ang II-induced hyperaldosteronism in mice. (A) The in-gel fluorescence imaging and target fishing assay for potential targets in adrenal tissue of mice. (B) The co-localization imaging of CYP11B2 and AAT-I in adrenal tissue of mice with fluorescence confocal microscopy. The pseudo-red color represents CYP11B2, the pseudo-green color represents AAT-I and the yellow merger represents CYP11B2 colocalized with AAT-I. Scale bar: 100 μ m. (C)–(H) The content of Na⁺, K⁺, and Cl⁻ in the serum and urine analyzed by an ion detection kit. (I)–(K) The content of ALD, Cort, and estradiol in the serum was analyzed with an ELISA kit. The mice in the negative control group were fed without treatment (Con). (L)–(N) The HR, SBP, and DBP of mice with aldosteronism after treatment. Hyperaldosteronism was induced in mice by Ang II (Mod) and treated with Spi (i.p., 20 mg/kg/day) or AT-I (i.p., 10, 20, 40 mg/kg/day) for one week. Data are expressed as means \pm SD ($n = 10$). #### $P < 0.001$ vs. Con; * $P < 0.05$, ** $P < 0.01$, *** $P < 0.001$ vs. Mod.

intended substrate^{51,52}. To our knowledge, AT-I is the first covalent inhibitor that blocks CYP11B2 by directly targeting the Cys450 residue.

In addition to CYP11B1, the inhibition of other steroid synthetases is a matter of concern with the clinical use of CYP11B2 inhibitors. Although other cytochrome P450s (e.g., CYP17A1 and CYP19A1) that produce steroids have low similarity to CYP11B2 (< 40%), inhibition of these P450s may have unintended consequences by affecting metabolic pathways leading to androgens and estrogens^{53–55}. For this reason, it is of utmost importance to evaluate the inhibitory effects on other steroidogenic cytochromes P450. It has been reported that AT-I may be a potential aromatase (CYP19A1) inhibitor *in vitro*⁵⁶. However, in the present study, both spironolactone and AT-I increased serum estradiol in the hyperaldosteronemic mice. The ability of spironolactone to increase the serum levels of estradiol in hyperaldosteronism in men has been reported⁵⁷. Our studies indicate that even if aromatase is inhibited by AT-I, AT-I will not aggravate the reduction of estrogens caused by hyperaldosteronism, although the mechanism is unclear. This is an advantage of AT-I, which is superior to other CYP11B2 inhibitors.

5. Conclusions

Our data demonstrates that Ala320 in CYP11B2 promotes the entry of AT-I into the catalytic pocket of CYP11B2, and the C8/C9 double bond of AT-I can be selectively epoxidated by CYP11B2 (but not by CYP11B1), and epoxidated AT-I covalently binds to the Cys450 of CYP11B2 to decrease the production of ALD and alleviate the symptoms of hyperaldosteronism. These studies will be useful for the design of a promising new drug class for the treatment of aldosterone-related cardiovascular diseases.

Acknowledgments

This study was supported by the National Key R&D Program of China (Nos. 2018YFC1704500 and 2018YFC1704505).

Author contributions

Gang Bai and Min Jiang designed the experiments and contributed to the review of the manuscript; Wenjuan Liu carried out the experiments, the data processing and information analysis, and wrote the manuscript; Zhenqiang Li synthesized AAT-I probe; Simeng Chu and Xiaoying Wang assisted with the animal experiments; Xiaoyao Ma performed the molecular docking experiments.

Conflicts of interest

The authors declare no conflicts of interest.

Appendix A. Supporting information

Supporting data to this article can be found online at <https://doi.org/10.1016/j.apsb.2021.09.013>.

References

- Bollag WB. Regulation of aldosterone synthesis and secretion. *Compr Physiol* 2014;**4**:1017–55.
- Yamazaki O, Ishizawa K, Hirohama D, Fujita T, Shibata S. Electrolyte transport in the renal collecting duct and its regulation by the renin-angiotensin-aldosterone system. *Clin Sci (Lond)* 2019;**133**:75–82.
- Schrier RW. Water and sodium retention in edematous disorders: role of vasopressin and aldosterone. *Am J Med* 2006;**119**:S47–53.
- Lalli E, Barhanin J, Zennaro MC, Warth R. Local control of aldosterone production and primary aldosteronism. *Trends Endocrinol Metab* 2016;**27**:123–31.
- Yang T, He M, Hu C. Regulation of aldosterone production by ion channels: from basal secretion to primary aldosteronism. *Biochim Biophys Acta Mol Basis Dis* 2018;**1864**:871–81.
- Seccia TM, Caroccia B, Gomez-Sanchez EP, Gomez-Sanchez CE, Rossi GP. The biology of normal zona glomerulosa and aldosterone-producing adenoma: pathological implications. *Endocr Rev* 2018;**39**:1029–56.
- Hellman DE, Kartchner M, Komar N, Mayes D, Pitt M. Hyperaldosteronism, hyperparathyroidism, medullary sponge kidneys, and hypertension. *JAMA* 1980;**244**:1351–3.
- Sowers JR, Whaley-Connell A, Epstein M. Narrative review: the emerging clinical implications of the role of aldosterone in the metabolic syndrome and resistant hypertension. *Ann Intern Med* 2009;**150**:776–83.
- Vaidya A, Mulatero P, Baudrand R, Adler GK. The expanding spectrum of primary aldosteronism: implications for diagnosis, pathogenesis, and treatment. *Endocr Rev* 2018;**39**:1057–88.
- Abad-Cardiel M, Alvarez-Alvarez B, Luque-Fernandez L, Fernandez C, Fernandez-Cruz A, Martell-Claros N. Hypertension caused by primary hyperaldosteronism: increased heart damage and cardiovascular risk. *Rev Esp Cardiol (Engl Ed)* 2013;**66**:47–52.
- Schrier RW, Masoumi A, Elhassan E. Aldosterone: role in edematous disorders, hypertension, chronic renal failure, and metabolic syndrome. *Clin J Am Soc Nephrol* 2010;**5**:1132–40.
- Whaley-Connell A, Johnson MS, Sowers JR. Aldosterone: role in the cardiometabolic syndrome and resistant hypertension. *Prog Cardiovasc Dis* 2010;**52**:401–9.
- Te Riet L, van Esch JH, Roks AJ, van den Meiracker AH, Danser AH. Hypertension: renin-angiotensin-aldosterone system alterations. *Circ Res* 2015;**116**:960–75.
- Burrello J, Buffolo F, Domenig O, Tetti M, Pecori A, Monticone S, et al. Renin-angiotensin-aldosterone system triple-a analysis for the screening of primary aldosteronism. *Hypertension* 2020;**75**:163–72.
- Funder JW. Aldosterone and mineralocorticoid receptors—physiology and pathophysiology. *Int J Mol Sci* 2017;**18**:1032.
- Sato A, Saruta T. Aldosterone escape during angiotensin-converting enzyme inhibitor therapy in essential hypertensive patients with left ventricular hypertrophy. *J Int Med Res* 2001;**29**:13–21.
- Schjoedt KJ, Andersen S, Rossing P, Tarnow L, Parving HH. Aldosterone escape during blockade of the renin-angiotensin-aldosterone system in diabetic nephropathy is associated with enhanced decline in glomerular filtration rate. *Diabetologia* 2004;**47**:1936–9.
- Pitt B, Zannad F, Remme WJ, Cody R, Castaigne A, Perez A, et al. The effect of spironolactone on morbidity and mortality in patients with severe heart failure. Randomized aldactone evaluation study investigators. *N Engl J Med* 1999;**341**:709–17.
- Barra-Chimal J, Girerd S, Jaisser F. Mineralocorticoid receptor antagonists and kidney diseases: pathophysiological basis. *Kidney Int* 2019;**96**:302–19.
- Rainey WE. Adrenal zonation: clues from 11 β -hydroxylase and aldosterone synthase. *Mol Cell Endocrinol* 1999;**151**:151–60.
- Schiffer L, Anderko S, Hannemann F, Eiden-Plach A, Bernhardt R. The CYP11B subfamily. *J Steroid Biochem Mol Biol* 2015;**151**:38–51.
- Santen RJ, Demers LM, Lynch J, Harvey H, Lipton A, Mulagha M, et al. Specificity of low dose fadrozole hydrochloride (CGS 16949A) as an aromatase inhibitor. *J Clin Endocrinol Metab* 1991;**73**:99–106.
- LaSala D, Shibanaka Y, Jeng AY. Coexpression of CYP11B2 or CYP11B1 with adrenodoxin and adrenodoxin reductase for assessing the potency and selectivity of aldosterone synthase inhibitors. *Anal Biochem* 2009;**394**:56–61.

24. Amar L, Azizi M, Menard J, Peyrard S, Watson C, Plouin PF. Aldosterone synthase inhibition with LCI699: a proof-of-concept study in patients with primary aldosteronism. *Hypertension* 2010;**56**:831–8.
25. Bertagna X, Pivonello R, Fleseriu M, Zhang Y, Robinson P, Taylor A, et al. LCI699, a potent 11 β -hydroxylase inhibitor, normalizes urinary cortisol in patients with cushing's disease: results from a multi-center, proof-of-concept study. *J Clin Endocrinol Metab* 2014;**99**:1375–83.
26. Zhu B, Zhang QL, Hua JW, Cheng WL, Qin LP. The traditional uses, phytochemistry, and pharmacology of *Atractylodes macrocephala* Koidz.: a review. *J Ethnopharmacol* 2018;**226**:143–67.
27. Xu S, Qi X, Liu Y, Liu Y, Lv X, Sun J, et al. UPLC–MS/MS of atractylenolide I, atractylenolide II, atractylenolide III, and atractyloside A in rat plasma after oral administration of raw and wheat bran-processed atractylodis rhizoma. *Molecules* 2018;**23**:3234.
28. Zhang W, Gao J, Cheng C, Zhang M, Liu W, Ma X, et al. Cinnamaldehyde enhances antimelanoma activity through covalently binding ENO1 and exhibits a promoting effect with dacarbazine. *Cancers (Basel)* 2020;**12**:311.
29. Dai J, Liang K, Zhao S, Jia W, Liu Y, Wu H, et al. Chemoproteomics reveals baicalin activates hepatic CPT1 to ameliorate diet-induced obesity and hepatic steatosis. *Proc Natl Acad Sci U S A* 2018;**115**:E5896–905.
30. Liu WJ, Chu GC, Chang NW, Ma XY, Jiang M, Bai G. Phillygenin attenuates inflammatory responses and influences glucose metabolic parameters by inhibiting Akt activity. *Rsc Adv* 2017;**7**:40418–26.
31. Hobler A, Kagawa N, Hutter MC, Hartmann MF, Wudy SA, Hannemann F, et al. Human aldosterone synthase: recombinant expression in *E. coli* and purification enables a detailed biochemical analysis of the protein on the molecular level. *J Steroid Biochem Mol Biol* 2012;**132**:57–65.
32. Cook DJ, Finnigan JD, Cook K, Black GW, Charnock SJ. Cytochromes P450: history, classes, catalytic mechanism, and industrial application. *Adv Protein Chem Struct Biol* 2016;**105**:105–26.
33. Zhang Y, Wang Z, Ma X, Yang S, Hu X, Tao J, et al. Glycyrrhetic acid binds to the conserved P-loop region and interferes with the interaction of RAS-effector proteins. *Acta Pharm Sin B* 2019;**9**:294–303.
34. Ershov PV, Yablokov EO, Florinskaya AV, Mezentsev YV, Kaluzhskiy LA, Tumilovich AM, et al. SPR-based study of affinity of cytochrome P450s/redox partners interactions modulated by steroidal substrates. *J Steroid Biochem Mol Biol* 2019;**187**:124–9.
35. Yablokov EO, Sushko TA, Kaluzhskiy LA, Kavaleuski AA, Mezentsev YV, Ershov PV, et al. Substrate-induced modulation of protein–protein interactions within human mitochondrial cytochrome P450-dependent system. *J Steroid Biochem Mol Biol* 2021;**208**:105793.
36. White PC. Disorders of aldosterone biosynthesis and action. *N Engl J Med* 1994;**331**:250–8.
37. Hamdane D, Zhang H, Hollenberg P. Oxygen activation by cytochrome P450 monooxygenase. *Photosynth Res* 2008;**98**:657–66.
38. Jung ST, Lauchli R, Arnold FH. Cytochrome P450: taming a wild type enzyme. *Curr Opin Biotechnol* 2011;**22**:809–17.
39. Bottner B, Bernhardt R. Changed ratios of glucocorticoids/mineralocorticoids caused by point mutations in the putative I-helix regions of CYP11B1 and CYP11B2. *Endocr Res* 1996;**22**:455–61.
40. Bottner B, Denner K, Bernhardt R. Conferring aldosterone synthesis to human CYP11B1 by replacing key amino acid residues with CYP11B2-specific ones. *Eur J Biochem* 1998;**252**:458–66.
41. Roumen L, Sanders MP, Pieterse K, Hilbers PA, Plate R, Custers E, et al. Construction of 3D models of the CYP11B family as a tool to predict ligand binding characteristics. *J Comput Aided Mol Des* 2007;**21**:455–71.
42. Schewe J, Seidel E, Forslund S, Marko L, Peters J, Muller DN, et al. Elevated aldosterone and blood pressure in a mouse model of familial hyperaldosteronism with CIC-2 mutation. *Nat Commun* 2019;**10**:5155.
43. Bernhardt R. The potential of targeting CYP11B. *Expert Opin Ther Targets* 2016;**20**:923–34.
44. Bogman K, Schwab D, Delporte ML, Palermo G, Amrein K, Mohr S, et al. Preclinical and early clinical profile of a highly selective and potent oral inhibitor of aldosterone synthase (CYP11B2). *Hypertension* 2017;**69**:189–96.
45. Brixius-Anderko S, Scott EE. Structure of human cortisol-producing cytochrome P450 11B1 bound to the breast cancer drug fadrozole provides insights for drug design. *J Biol Chem* 2019;**294**:453–60.
46. Schroer K, Kittelmann M, Lutz S. Recombinant human cytochrome P450 monooxygenases for drug metabolite synthesis. *Biotechnol Bioeng* 2010;**106**:699–706.
47. Strushkevich N, Gilep AA, Shen L, Arrowsmith CH, Edwards AM, Usanov SA, et al. Structural insights into aldosterone synthase substrate specificity and targeted inhibition. *Mol Endocrinol* 2013;**27**:315–24.
48. Belkina NV, Lisurek M, Ivanov AS, Bernhardt R. Modelling of three-dimensional structures of cytochromes P450 11B1 and 11B2. *J Inorg Biochem* 2001;**87**:197–207.
49. Kang P, Liao M, Wester MR, Leeder JS, Pearce RE, Correia MA. CYP3A4-mediated carbamazepine (CBZ) metabolism: formation of a covalent CBZ–CYP3A4 adduct and alteration of the enzyme kinetic profile. *Drug Metab Dispos* 2008;**36**:490–9.
50. Ma X, Zhang Y, Wang Z, Shen Y, Zhang M, Nie Q, et al. Ursolic acid, a natural nutraceutical agent, targets caspase3 and alleviates inflammation-associated downstream signal transduction. *Mol Nutr Food Res* 2017;**61**:1700332.
51. Sakakibara R, Sasaki W, Onda Y, Yamaguchi M, Ushiroguchi H, Hiraga Y, et al. Discovery of novel pyrazole-based selective aldosterone synthase (CYP11B2) inhibitors: a new template to coordinate the heme-iron motif of CYP11B2. *J Med Chem* 2018;**61**:5594–608.
52. Sparks SM, Danger DP, Hoekstra WJ, Leesnitzer T, Schotzinger RJ, Yates CM, et al. Development of highly selective pyrimidine-based aldosterone synthase (CYP11B2) inhibitors. *ACS Med Chem Lett* 2019;**10**:1056–60.
53. Cerny MA. Progress towards clinically useful aldosterone synthase inhibitors. *Curr Top Med Chem* 2013;**13**:1385–401.
54. Boden WE, Miller MG, McBride R, Harvey C, Snabes MC, Schmidt J, et al. Testosterone concentrations and risk of cardiovascular events in androgen-deficient men with atherosclerotic cardiovascular disease. *Am Heart J* 2020;**224**:65–76.
55. Caroccia B, Seccia TM, Barton M, Rossi GP. Estrogen signaling in the adrenal cortex: implications for blood pressure sex differences. *Hypertension* 2016;**68**:840–8.
56. Jiang H, Shi J, Li Y. Screening for compounds with aromatase inhibiting activities from *Atractylodes macrocephala* Koidz. *Molecules* 2011;**16**:3146–51.
57. Rose LI, Underwood RH, Newmark SR, Kisch ES, Williams GH. Pathophysiology of spironolactone-induced gynecomastia. *Ann Intern Med* 1977;**87**:398–403.